

Room Temperature Excitons in BaCuChF

Senior Thesis

Oregon State University

June 14, 2007

Joseph Kinney

Research Advisor: Janet Tate

Abstract

The family of transparent p-type semiconductors BaCuChF (Ch= S, Se, and Te) have potential application in the field of transparent electronics due to a current lack of transparent p-type materials. Excitonic peaks are observed near the band edge in BaCuSeF and BaCuTeF films under room temperature conditions. The presence of excitons at room temperature implies that the binding energy of these excitons is larger than 25 meV. The bandgap in these materials is between 3-3.5 eV. The excitons in these materials could be used to create optoelectronic devices that operate in the ultraviolet region of the spectrum. BaCuTeF was also examined and did not display any excitonic peaks. Absorption spectra measured from room temperature down to 80 K were obtained for all three materials, BaCuSF, BaCuSeF, and BaCuTeF.

Contents

1	Introduction	3
2	Background	4
2.1	Absorption in Semiconductors	4
2.2	Excitons	5
2.3	BaCuChF	8
2.4	LnCuOCh and ZnO	9
3	Experimental Method	10
3.1	Spectrometer	10
3.2	Thin Film Interference	14
3.3	Cryostat	16
3.4	Measurement Procedure	17
3.4.1	Operation of K-77 temperature controller	18
3.4.2	Cool down procedure	19
3.4.3	Warm up procedure	21
4	Results and Analysis	22
5	Conclusion	29
6	Acknowledgments	30
A	The hydrogen atom in two dimensions	31

1 Introduction

What if someone could make a computer chip that was as clear as a pane of glass? This property would allow all kinds of interesting devices to be created. BaCuChF (Ch =chalcogen) is a transparent semiconductor which could be used to make just such a device.

A transparent semiconductor is a material that can be used to make complex circuits and devices, which let light pass straight through. Having a material that is transparent, yet is still a semiconductor, opens up a world of applications that would be impossible with a typical semiconductor. A few possible applications for transparent semiconductors are controlling the pixels on a monitor, building electronics into the windshield of a car, or making a portable device that appears to be nothing but a screen. A current challenge facing the field of transparent semiconductors is finding materials that are of the right type. There is a wide base of work on n -type transparent semiconductors and a number of useful devices have been made using just n -type materials [1, 2]. However, there is presently a lack of p -type transparent semiconductors. In order to obtain full functionality, similar to what typical non-transparent semiconductors can produce, both p -type and n -type materials are needed. The material BaCuChF is a p -type transparent semiconductor that could be used to provide the complementary functionality that is currently missing.

Potential application as a transparent p -type semiconductor is the primary, but not the only, reason for studying the material BaCuChF. In addition to being a p -type semiconductor, BaCuChF also displays some interesting optical properties, namely room temperature excitons. The study of room temperature excitons is the focus of this thesis. An exciton is a bound state between a hole and an excited electron in a semiconductor. An exciton occurs when an excited electron still feels the positive charge of the hole and the two particles, electron and hole, are bound together. An exciton can be useful in optical applications because photons are absorbed when the electron is excited into the exciton state and light is

emitted when the electron relaxes out of the exciton state. This creation of light can be used to make devices like LEDs and laser diodes. Excitons have been studied in many materials, but generally these experiments must be performed at very cold temperatures, around 4 K. The excitons displayed in BaCuChF exist under room temperature conditions and occur at ultraviolet wavelengths. One possible application for using the exciton in BaCuChF would be to build an ultraviolet LED.

2 Background

2.1 Absorption in Semiconductors

Semiconductors are the basis of the modern electronics industry, diodes, transistors, etc. How these materials interact with light gives insight into the properties of the material, namely the band structure where electrons and holes live. A semiconductor, doped silicon for example, is defined as a material with a room temperature resistivity of 10^{-2} to 10^9 ohm-cm. Copper, a typical metal, has a resistivity of 5.88×10^{-6} ohm-cm [3]. A key difference between a metal and a semiconductor is that in a semiconductor there is an energy bandgap between the highest occupied energy band, called the valence band, and the lowest unoccupied energy band, called the conduction band. In a semiconductor the valence band is entirely filled and the conduction band is empty. In a metal the conduction band is a partially full band, meaning that for an electron to move to an excited conducting state it only needs an infinitesimal amount of energy. In a semiconductor an electron must absorb energy equal to or greater than the bandgap of the material to excite that electron to a state in the conduction band. A photon of energy less than the bandgap of the semiconductor will pass through that material unaffected. Using this information one can determine the band gap of a semiconductor by measuring the absorption of the semiconductor for different energies of light. Fig. 1 shows an absorption spectrum for the semiconductor BaCuTeF,

in the vicinity of the bandgap. At energies larger than the bandgap absorption steadily increases, while at energies less than the bandgap absorption is low. An exciton state would appear in the absorption spectrum as an additional peak at energies just below the bandgap.

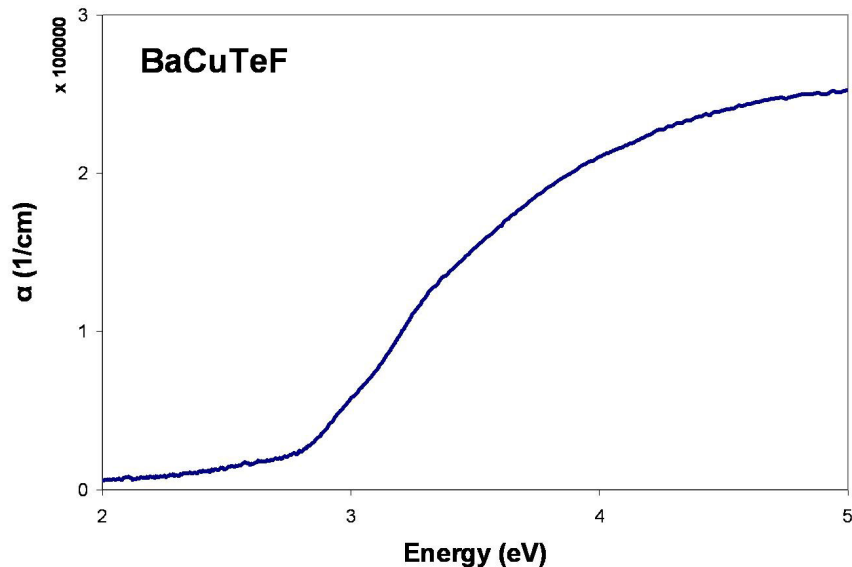


Figure 1: Absorption spectrum for a thin film of BaCuTeF. The bandgap for this material is at 2.9 eV. The thickness of this sample is 150 nm.

2.2 Excitons

An exciton is a bound state of a hole and an electron. A hole is a lack of an electron. A hole describes a large group of electrons by the one missing electron. In many ways an exciton is similar to a hydrogen atom, both a hydrogen atom and an exciton consist of a positive and a negative charge bound together by a Coulomb attraction. Because an exciton is similar to a hydrogen atom, one can use a hydrogen like model to predict the energy states of an exciton.

$$E(n) = E_{gap} - \frac{R^*}{n^2} \quad (1)$$

$$n = 1, 2, \dots$$

[4]. This model assumes the electron and hole have a relatively large spacing between them, many lattice constants, and this type of exciton is referred to as a Wannier exciton [5]. The alternate model assumes that the electron is bound to a single lattice point in the crystal and was developed by Frenckel. Those excitons are called Frenckel excitons. For the Wannier, hydrogen like model, the energy states vary like $\frac{1}{n^2}$ and are shifted by the bandgap of the semiconductor to account for the condition that an electron in a semiconductor is considered free when it has a bandgap worth of energy. R^* is an effective Rydberg constant, a measure of the binding energy of the exciton. For a hydrogen atom the binding energy $R = 13.6eV$, the amount of energy required to ionize an electron from the ground state. R^* is defined as

$$R^* = \frac{\mu e^4}{2\hbar^2(4\pi\epsilon_0)^2\epsilon_r^2} = \left(\frac{\mu}{m\epsilon_r^2}\right) \times 13.6eV \quad (2)$$

[4], where \hbar is Plank's constant divided by 2π , ϵ_0 is the permativity of free space, m_e is the mass of the electron, ϵ_r is the relative dielectric constant inside the semiconductor, and μ is the reduced mass combination of the hole and electron is defined as

$$\frac{1}{\mu} = \frac{1}{m_e^*} + \frac{1}{m_h^*} \quad (3)$$

where m_e^* and m_h^* are the effective masses of the electron and hole inside the semiconductor. The reduced mass is used because the effective mass of the electron and hole are of nearly the same magnitude, unlike a hydrogen atom where the mass of the proton is much larger than the mass of the electron.

The previous discussion assumes a hydrogen like model for the exciton where the hole and electron are free to move in 3 dimensions. The material BaCuChF has a layered structure where the holes and electron are confined to 2 dimensional layers of the material. This

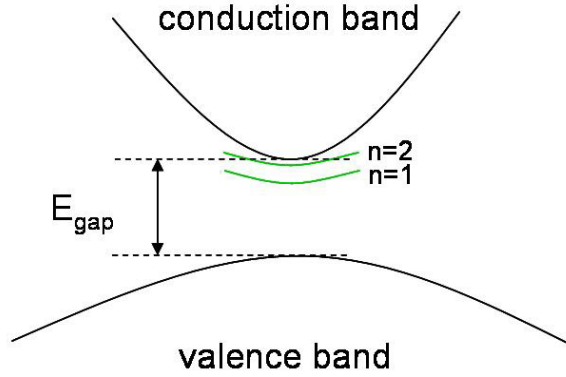


Figure 2: Schematic diagram of the bandgap in a semiconductor including sub bandgap exciton states.

confinement changes the energy spacings of exciton levels, instead producing the result

$$E(n) = E_{gap} - \frac{R^*}{(n - \frac{1}{2})^2} \quad (4)$$

where R^* and n have the same meaning as before. This result is worked out in mathematical detail in appendix A.

Room temperature excitons are the study of this thesis, both BaCuSF and BaCuSeF samples display exciton features at room temperature. An exciton must have a binding energy of 25 meV or larger to be observed in room temperature measurements, 25 meV corresponds to $k_B T$, the available thermal energy at 300 K. Excitons have been studied in a wide variety of materials over the years. Generally these measurements are done at very low temperatures due to the fact that the binding energies of the excitons are very small. Some examples of materials with small binding energies are GaP, Ge, and GaAs with binding energies of 3.5 meV, 4.15 meV, and 4.2 meV respectively [3]. In order to observe excitons in these materials, measurements must be performed at temperatures of 4 K or less. Some notable exceptions to this small binding energy rule are alkali halides, KCl and KI being two

examples, with binding energies of 400 meV and 480 meV [3].

2.3 BaCuChF

The material studied for this thesis was BaCuChF, where the chalcogens (Ch) used were the group six elements sulfur (S), selenium (Se), and tellurium (Te). Two unique properties displayed by BaCuChF are transparent p -type conductivity and room temperature excitons making these materials particularly well suited toward applications in the areas of transparent electronics and optoelectronics.

In the area of transparent electronics n -type devices have been constructed and demonstrated with great success [1, 2]. The same cannot be said for transparent p -type materials which have been harder to come by. In order to create a complementary CMOS logic entirely out of transparent materials, both p -type and n -type materials are needed. BaCuChF is a p -type transparent semiconductor that could fill this need. Fabrication techniques and electrical properties of BaCuSeF and BaCuSF can be found in work done by Janet Tate's group here at OSU [6, 7].

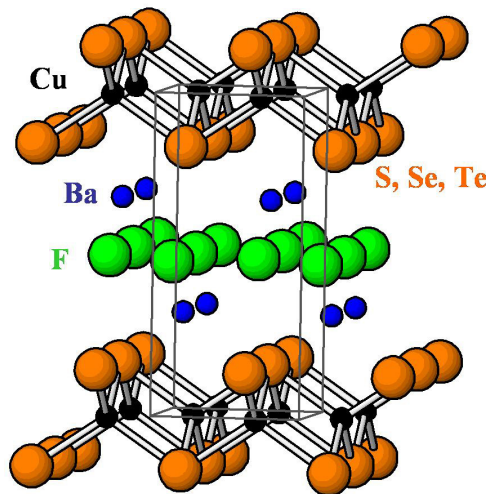


Figure 3: Diagram of lattice structure of BaCuChF. Alternating layers of insulating $(\text{Ba}_2\text{F}_2)^{2+}$ and hole conductive $(\text{Cu}_2\text{Ch}_2)^{2-}$ form a quantum well structure confining exciton to two dimensions.

Both unique properties, transparent p -type conductivity and room temperature excitons, can be attributed, in part, to the layered crystal structure of BaCuChF. As can be seen from Fig. 3, BaCuChF is composed of alternating layers of $(\text{Ba}_2\text{F}_2)^{2+}$ and $(\text{Cu}_2\text{Ch}_2)^{2-}$. Taken separately, BaF₂ is a wide gap (9.1 eV) insulating material and Cu₂Ch is a narrow gap (1.2-2.2 eV) p -type semiconductor. Combining these two materials has the effect of creating a p -type semiconductor with a wide bandgap. The wide bandgap means that the material is transparent to visible light. Coupling this wide bandgap with the hole conductivity of the Cu₂Ch layers produces a transparent p -type semiconductor. The layered structure allows the conflicting properties of conduction and insulation to coexist in the same material.

Each Cu₂Ch layer is surrounded on top and bottom by an insulating BaF₂ layer. This type of structure on a larger scale is often referred to as a quantum well. The Cu₂Ch layer is where conduction is taking place and it is fair to say that the charge carriers are confined to the two dimensional region formed by this layer. This confinement means that the electron and hole forming an exciton are forced together and consequently are bound together more tightly. The two dimensional quantum well nature of BaCuChF produces excitons with increased binding energies contributing to the fact that excitons can be observed at room temperature in samples of BaCuChF. This concept was demonstrated using GaAs quantum wells, wires, and dots. Each decrease in dimensionality produced an increase in the binding energy [8].

2.4 LnCuOCh and ZnO

It is unusual to see excitons under room temperature conditions, as is the case for BaCuChF. However BaCuChF is not the first material to display this property. Notable examples are LnCuOCh (Ln =lanthanide, Ch =chalcogen), and ZnO.

The material LnCuOCh is similar to BaCuChF both in chemical structure and physical properties. For these reasons previous work on the material LnCuOCh was used as a guide

for the research presented in this thesis. Like BaCuChF, LnCuOCh is a transparent *p*-type semiconductor, and LnCuOCh samples also display room temperature excitons. Room temperature excitons were observed in LaCuOS samples, which has a bandgap of 3.1 eV, putting these features in the ultraviolet region of the spectrum [9]. Other work performed on LnCuOCh showed multiple exciton peaks at the band edge. The splitting of the exciton peaks was attributed to spin orbit interactions and the magnitude of the splitting was shown to increase or decrease depending on the lanthanide (La, Pr, or Nd) or chalcogen (S, Se, or Te) used to form the material [10].

ZnO also displays excitonic features at room temperature. ZnO has been studied extensively over the past 50 years. The earliest studies of excitons in ZnO were performed by Thomas in 1960 [11] and Park in 1966 [12]. Three exciton series are observed in ZnO with binding energies of 42 meV, 41 meV, and 38 meV [12].

3 Experimental Method

3.1 Spectrometer

A grating spectrometer was used to obtain absorption spectra of BaCuChF films. There are three components to a spectrometer system, light source, wavelength isolator, and detector. For these experiments a Xe arc lamp was used for the light source, a double grating monochromator was used to isolate wavelengths, and a silicon photodiode was the detector.

The exciton features appear at wavelength between 310-413 nm (3-4eV), in the ultraviolet region of the spectrum. Therefore, it was important that all components of the spectrometer function properly in the UV region of the spectrum. The Xe arc lamp produces a wide spectrum of light that extends into the UV. Fig. 5 shows the lamp spectrum for both a Xe arc lamp and a tungsten halogen lamp, the two different sources available. The Xe arc lamp produces a stronger signal farther into the UV region, making it the best choice for

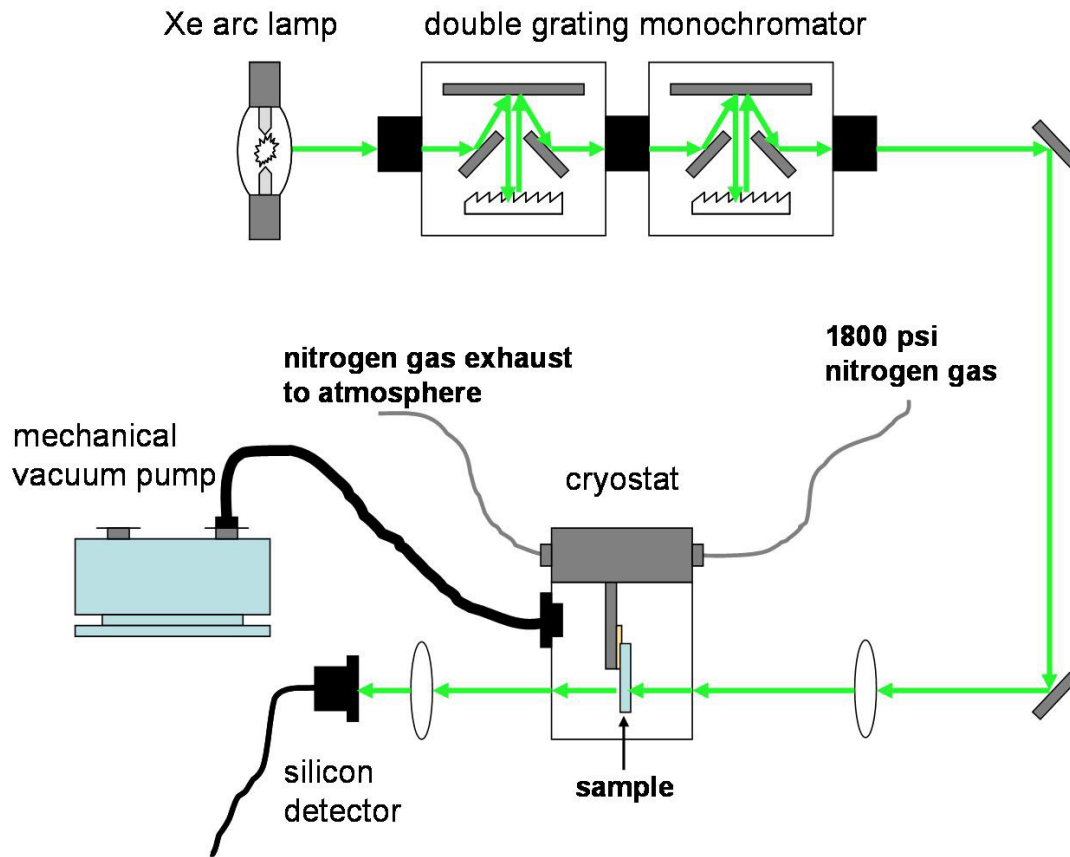


Figure 4: Experimental apparatus used to measure the absorption coefficient of thin films of BaCuChF at temperatures from 80 K up to room temperature. These measurements required the combination of an optical cryostat with a grating spectrometer.

measurements of excitons in BaCuChF. For light produced by the Xe arc lamp the lower wavelength limit is set by oxygen absorption in air which cuts off wavelengths of 180 nm or smaller. For wavelengths larger than 180nm the Xe arc lamp is a good source.

The second component of the spectrometer system was a double monochromator. The gratings used in the double monochromator were blazed to have a maximum efficiency at 250 nm. This optimized the signal for the wavelength region where exciton features were observed. The final piece of the spectrometer system was a silicon photodiode detector. The Si detector is effective in the wavelength range of 200-1000 nm. All the components of the

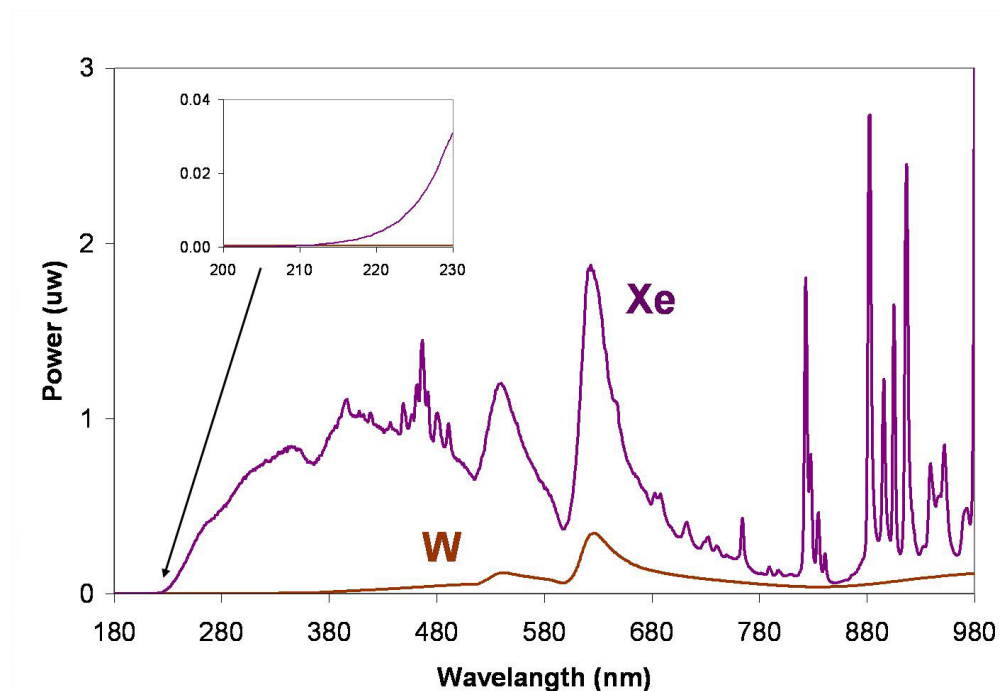


Figure 5: Spectrum for the two available lamp sources. The tungsten (W) halogen lamp is more stable over a wide range of wavelengths, but the Xe arc lamp produces a stronger signal into the UV region of the spectrum.

spectrometer where optimized to produce the highest quality measurement possible in the UV region of the spectrum. The measured signal to noise ratio at 330 nm was 100:1.

In addition to making sure that there was adequate signal at UV wavelengths it also was important to determine the resolution of the spectrometer. The exciton features appear as peaks in the absorption spectrum and knowing the minimum resolution of the spectrometer determined the minimum peak width that could be resolved by the spectrometer. For low temperature measurements, where the peak becomes sharpest, measured peak widths approached the minimum resolution of the spectrometer. The resolution of the spectrometer is controlled by the width of the input and output slits of the double monochromator. For the measurements presented here, both the input and output slits had a width of 0.76 mm, which would produce an expected minimum resolution of 5 nm when used in a single monochromator with a grating line density of 1200 lines/mm at an input wavelength of 500

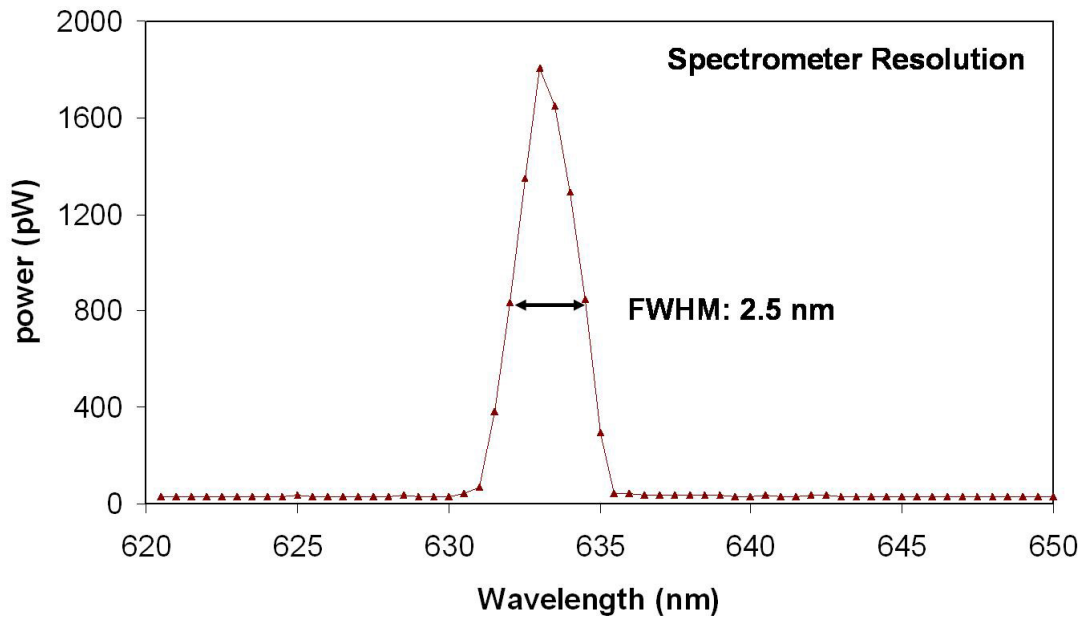


Figure 6: Spectrum of a HeNe laser. The actual linewidth of the HeNe laser is much smaller than the resolution of the spectrometer, so the width plotted here gives an accurate measure of the minimum resolution of the spectrometer. Slit widths of 0.76 mm were used at the entrance and exit of a double monochromator, and the measured full width at the half power point is 2.5 nm.

nm. In the case of a double monochromator this resolution is cut in half, giving an expected resolution of 2.5 nm. This resolution was verified by measuring the spectral linewidth of a HeNe laser, shown in Fig. 6. The typical linewidth of a HeNe laser is a few picometers, while the resolution of the spectrometer is three orders of magnitude larger at a few nanometers. Therefore, the width of the HeNe measured by the spectrometer gives an accurate measurement of the minimum resolution of the spectrometer. The FWHM from the peak in Fig. 6 confirms that the resolution of the spectrometer is 2.5 nm, which agrees with the expected value based on the monochromator components. The sharpest exciton peak measured had a width of 0.026 eV which corresponds to a linewidth of 3.2 nm. This linewidth is near the minimum resolution of the spectrometer meaning that the sharpest peaks measured were approaching the resolution limit of the spectrometer.

3.2 Thin Film Interference

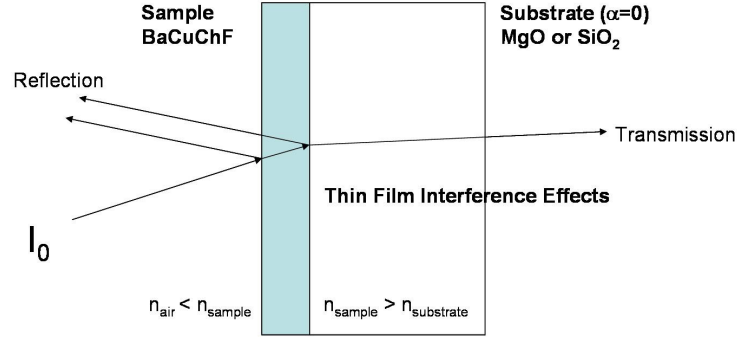


Figure 7: Illustration of interference effect that occurs in the transmission and reflection spectra when the sample is a thin film.

Useful interference effects occur when the material deposited is a thin film. A thin film is defined as a film with a thickness in the range of 100-1000 nm, roughly the same order as the wavelength of visible light. This condition means that a broadband light source, like the Xe arc lamp used for these experiments, will be coherent over this distance and light reflecting from the back surface can interfere destructively or constructively with the reflection from the front surface based on the conditions

$$m\lambda = 2nd \quad (5)$$

$$m = \frac{1}{2}, \frac{3}{2}, \frac{5}{2} \dots \text{maximum in R}$$

$$m = 1, 2, 3 \dots \text{minimum in R}$$

. In this equation λ is the wavelength of the incident light, n is the index of refraction of the material, and d is the thickness of the film. The conditions for m to produce constructive or destructive interference were determined assuming that the sample has a larger index of refraction than the substrate, which is the case for the materials presented in this thesis. A

π phase shift occurs at the front surface where the light passes from the low index air to the high index sample and no phase shift occurs at the back surface where the light passes from the high index sample to the lower index substrate. A maximum or minimum in the transmission signal will occur under the opposite conditions as a maximum or minimum for reflections. The transmitted signal is simply the leftover signal that does not get reflected or absorbed, so it follows that when the interference condition maximizes the reflected signal this will produce a minimum in the transmitted signal.

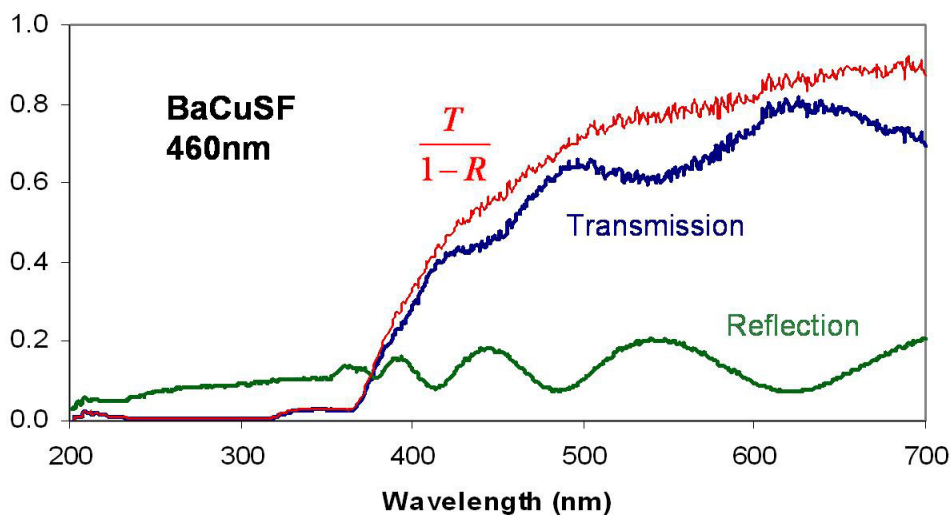


Figure 8: Typical optical measurement of a thin film of BaCuSF, thickness 460 nm, showing interference fringes in both the transmittance and reflectance. Also plotted is the interference free transmission $\frac{T}{1-R}$.

Fig. 8 displays a typical set of transmission and reflection data, showing interference fringes in both T and R . Here T is the transmittance and R is the reflectance, both quantities have been normalized relative to the input lamp signal. The other plotted quantity $\frac{T}{1-R}$ is considered the interference-free transmission or the transmission normalized relative to the reflection. There are no interference fringes in $\frac{T}{1-R}$ because a minimum in reflection corresponds to a maximum in transmission and these two effects cancel out when R and T are combined in the fraction $\frac{T}{1-R}$.

Another way to think about this quantity $\frac{T}{1-R}$ is to consider the absorption of the material. Absorption spectra are the primary tool used in this thesis for detailing exciton states in BaCuChF and the absorption coefficient α can be determined from $\frac{T}{1-R}$ and the film thickness d through the relationship

$$(1 - R)e^{-\alpha d} = T \quad (6)$$

3.3 Cryostat

An optical cryostat was used to measure absorption spectra for BaCuChF at temperatures down to 80 degrees Kelvin. The cryostat used was MMR's Optical Transmission System and is pictured in Fig. 9. This cryostat makes use of the Joule Thomson effect, namely that a gas expanding at constant enthalpy cools.

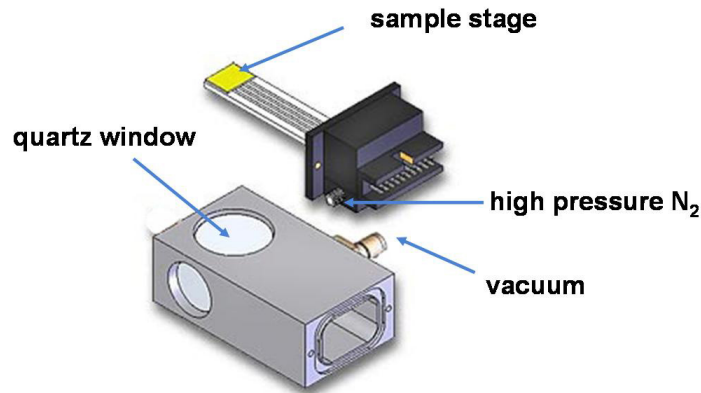


Figure 9: Optical cryostat used for low temperature transmission measurements. This image was adapted from MMR's web page (<http://mmr.com/optical.html>).

High pressure nitrogen gas at 1800 psi was used to cool a copper mounting plate to a minimum temperature of 80 K. The minimum temperature is limited by the boiling temperature of nitrogen. High purity nitrogen gas was required for the cryostat to function properly.

Grade 3.8 (Pre-purified Grade) nitrogen gas was passed through a filter which removed hydrocarbons and water to minimize the possibility of clogging. The gas is required to pass through a series of thin capillary tubes during the cooling process and a small amount of water can freeze in the tubes, clogging up the flow of gas and stopping the cooling process. The copper cooling plate was surrounded by a vacuum chamber pumped down to 5 mtorr with the purpose of insulating the 80 K cooling plate from the ambient environment. Quartz windows on the front and back of the vacuum chamber allowed light from the spectrometer to pass into the cryostat, through the cooled sample, and out again to be measured. The sample was mounted on the cold copper plate using Apeizon N grease. Apeizon N grease is designed to be a good thermal conductor at low pressure, making it ideal for this application.

A diode and 100 Ω resistor were wired inside the cooling stage. The purpose of the diode was to measure the temperature of the copper plate and sample. The resistor acted as a heater allowing the temperature of the plate to be adjusted. Both resistor and diode were wired into a K-77 temperature control circuit allowing the temperature of the sample to be set and held at any temperature in the range from 80 K up to 373 K (100 °C).

3.4 Measurement Procedure

The primary measurements made for this thesis were absorption spectra taken at low temperatures showing exciton states in BaCuSF and BaCuSeF. Two separate pieces of information are needed to determine the functional dependence of the absorption coefficient (α) on energy, the thickness of the film and the transmittance of the film as a function of wavelength (λ), at a particular temperature. The thickness of the film was determined by measuring transmission and reflection at room temperature. This measurement was done without the use of the cryostat because the windows on the cryostat add additional reflections which cannot be entirely separated from the desired reflection measurement. Levi Kilcher's senior thesis provides a comprehensive discussion on the details of operating the spectrometer to

measure transmission and reflection, as well as how to fit this data to determine the thickness of a film. These details will not be repeated here. Instead I will focus on the low temperature measurements that involved the operation of the cryostat.

3.4.1 Operation of K-77 temperature controller

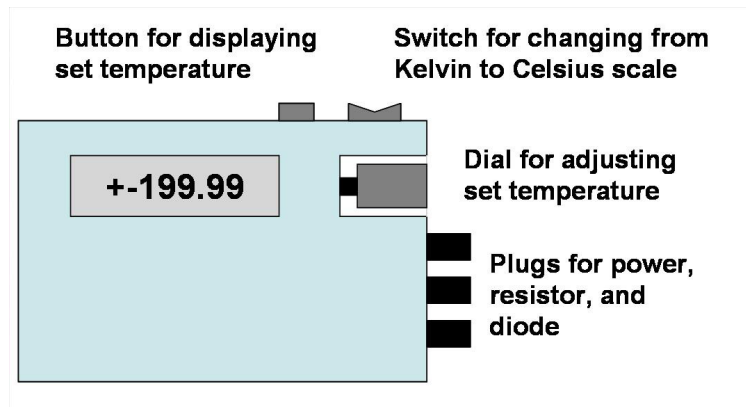


Figure 10: K-77 temperature controller used to both read and control the temperature of the cold stage of the optical cryostat.

A diagram of the connections and controls of the K-77 controller is shown in Fig. 10. The two components that are controlled by the K-77 are a diode and resistor both of which are located inside the cooling stage of the cryostat. The diode measures the temperature of the cold stage and receives power from a 9 V battery located inside the K-77, accessed by unscrewing the back. The second component controlled by the K-77 is a resistor that acts as a heater. The resistor receives power from a transformer plugged into an outlet and connected into the side of the K-77. Because the two components have separate power supplies they can operate more or less independently.

The temperature is read with the diode by flipping the switch on top of the K-77 to either the Celsius or Kelvin setting. Both settings are needed because the display screen is limited to a range of ± 199 . This means that room temperature (293 K) will be out of range on the Kelvin scale and the K-77 will display a positive one followed by blanks in the other digits,

indicating the temperature is too large for the current scale. If the actual temperature is too small the display will read a negative one followed by blanks. Connectivity of the diode can be verified by measuring the resistance across the two connections on the diode plug with a multimeter. In one direction the diode will have a very large resistance and in the opposite direction the resistance will measure around $500\text{ k}\Omega$.

The connectivity of the resistor can be verified in a similar way. It should read $100\ \Omega$ in either direction. The resistor is used to set the temperature to a point besides 80 K. This is done by changing the set temperature on the K-77 controller. Pressing the button on top of the K-77 will display the set temp which can then be adjusted by turning the large black dial. The K-77 controller will run current through the resistor whenever the set temperature is higher than the measured temperature, heating the stage up to the set temperature.

3.4.2 Cool down procedure

- Turn on the Xe arc lamp and let it warm up and stabilize for 30 minutes.
- Mount the sample on the copper cooling plate of the cryostat using Apeizon N grease. Line up the cryostat so the light passes through the sample and is not partially blocked by the copper mounting plate of the cryostat. Secure the cryostat by screwing it down to the optics table.
- Hook the vacuum line to the cryostat and mechanical vacuum pump. This line will have a tendency to want to pull the cryostat around, so it is best to make sure the cryostat is lined up properly and secured before connecting the vacuum line. Also make sure that the thin, stainless steel high pressure gas line is connected to the cryostat. The high pressure nitrogen line should never be disconnected because exposing the line to the air will allow moisture into the system which will freeze inside the cryostat and keep it from cooling properly.

- Measure the lamp spectrum with the cryostat in place but with the sample removed, keep the sample mounted on the cooling plate and remove the entire cooling plate. It is important to have the light signal pass through the windows of the cryostat when making a baseline lamp measurement. The windows of the cryostat add an additional effect to the reflection and transmission signals. By measuring the lamp signal with the cryostat windows in place, one can then divide out the effect of the windows to obtain reflectance and transmittance values.
- After a lamp spectrum has been taken, replace the cooling stage with the attached sample and seal it into the cryostat.
- Turn on the vacuum pump and allow it to pump out the cryostat chamber for 30 minutes. There is no vacuum gauge on the vacuum line because I wanted to limit the number of connections and potential leak points in the vacuum system. One simple way to determine if the vacuum is good is to listen to the pump. Ideally, the pump will sputter and spit for a minute or two when first turned on but should then run smoothly making a steady hum.
- Turn the high pressure gas line on at 500 psi for one minute. This is not enough pressure to cool the cryostat and will instead serve to flush out any moisture or impurities that may be residing in the cryostat.
- Make sure the set temperature on the K-77 is at 80 K. This will allow the cryostat to cool down to 80 K without being interrupted by the resistor heater. After 80 K has been reached the set temperature can be changed to heat up to the desired temperature for measurements.
- Turn the high pressure gas line on at 1800 psi to begin the cool down process. The temperature can be monitored on the K-77 temperature controller and the gas flow

can be monitored on the flowmeter connected to the exhaust nitrogen gas line. The temperature will typically cool down from room temp to 80 K in 15-20 min. Typical flowmeter readings are 3-4 when the gas is first turned and should steadily increase to 3.5-4.5 as the cryostat cools down. At 80K the flow meter will jump wildly because the temperature is cold enough for the nitrogen gas to condense in the line temporarily and block the flow.

Once the desired temperature has been reached measure the transmission and/or reflection spectra. For the data presented in this thesis only transmission was measured. This minimized the time spent at temperatures below freezing where there was a potential for ice building up on the sample due to moisture inside the cryostat chamber from an imperfect vacuum. Absorption was large in the region of the spectrum where excitons were observed and measuring reflection would cause only a small vertical shift to the presented data.

3.4.3 Warm up procedure

- Turn off the high pressure nitrogen gas. Both the gauge on the gas tank and the flow meter on the nitrogen exhaust will slowly go to zero after the gas has been turned off.
- Set the K-77 to room temperature (20 °C). This will speed up the warm up process.
- Once the temperature reads room temperature leave it there for 20 min. This will allow the entire system to reach room temperature.
- Vent the vacuum chamber with nitrogen gas. Only a very low pressure of nitrogen is needed, set the regulator from the high pressure tank as low as possible that will still let out a little gas. Sending 1800 psi into the vacuum chamber would be a bad idea. The vacuum pump should still be running at this point. Turning the pump off while the chamber is still under vacuum will pull oil from the pump into the vacuum chamber.

- Turn off the vacuum pump when the chamber is back to atmospheric pressure. The pressure can be determined by watching the vacuum pump. The pump will exhaust a solid cloud of oil when it is pumping on atmosphere.
- Turn off the venting nitrogen gas.
- Remove the sample and wipe off Apiezon N grease. I have found that the Apiezon N grease comes off easily and only needs a good wipe with a Kimwipe.

4 Results and Analysis

Measurements of the absorption coefficient at a range of temperatures from 80 K up to room temperature are presented for three different compounds, BaCuSeF, BaCuSF, and BaCuTeF, in Figures 11-13.

The absorption coefficient was calculated from transmission measurements using the formula

$$\alpha = -\frac{\ln(T)}{d} \quad (7)$$

. Where d , the thickness of the film, was determined by fitting the fringes in room temperature reflection and transmission data. I did not measure reflection at low temperature for two reasons. The windows of the cryostat create extra reflections that cannot be separated from the reflection of the film. The second reason for measuring only transmission was to minimize the time spent below freezing. Water vapor not entirely evacuated from the inside of the cryostat slowly builds up on the sample during the time the sample spent below freezing. This creates a film of water on top of the sample with its own reflection and transmission that will distort the measurement.

The absorption coefficient from the BaCuSeF sample shows two distinct excitonic peaks at 3.11 eV and 3.25 eV, when measured at 80 K. In the BaCuSF sample there are three

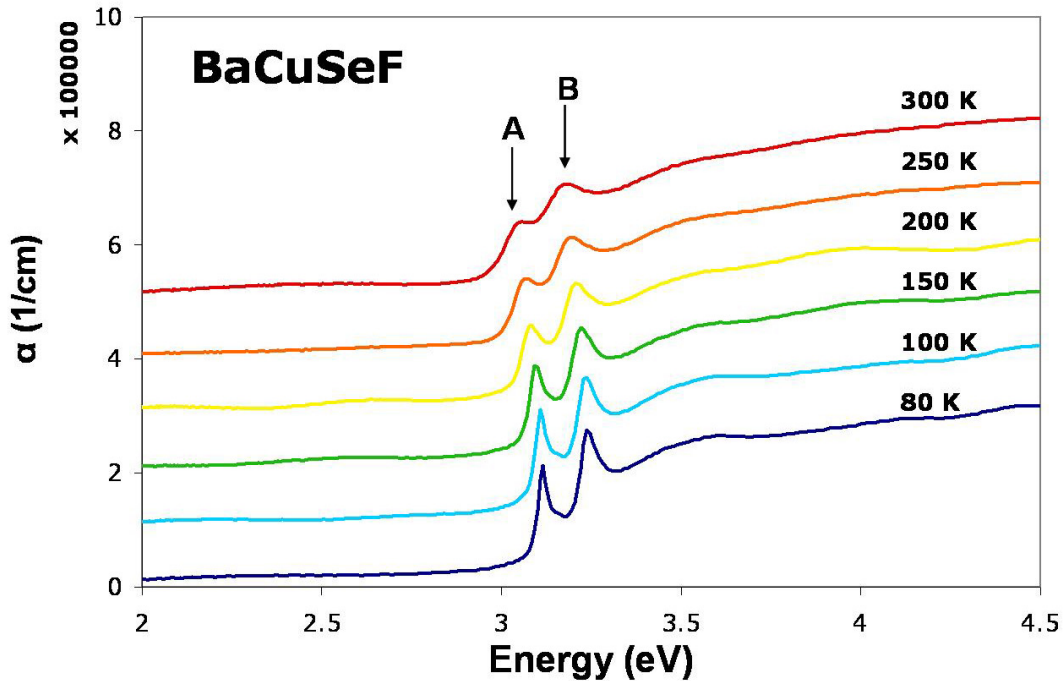


Figure 11: Absorption spectra for a thin film of BaCuSeF grown on an MgO substrate. Spectra were taken at a range of temperatures from 300 degrees Kelvin down to 80 degrees Kelvin. The spectrum at each temperature is shifted vertically for clarity. (Sample #10, $d = 180$ nm)

peaks, a pair at 3.31 eV and 3.34 eV, and a third peak at 3.88 eV. For both BaCuSeF and BaCuSF the exciton features appear in the ultraviolet region of the spectrum near 3.1 eV (400 nm). The BaCuTeF sample shows a sharp increase in absorption associated with the bandgap of the material, but there are no peaks in the absorption spectrum when measured at 80 K. It is possible that measurements at even lower temperatures would show excitonic features in BaCuTeF.

The exciton peaks in all samples shift to higher energies when measured at lower temperatures. The shift in location of the exciton peaks parallels the expected shift of the bandgap with changes in temperature. The temperature dependence of the bandgap can be modeled

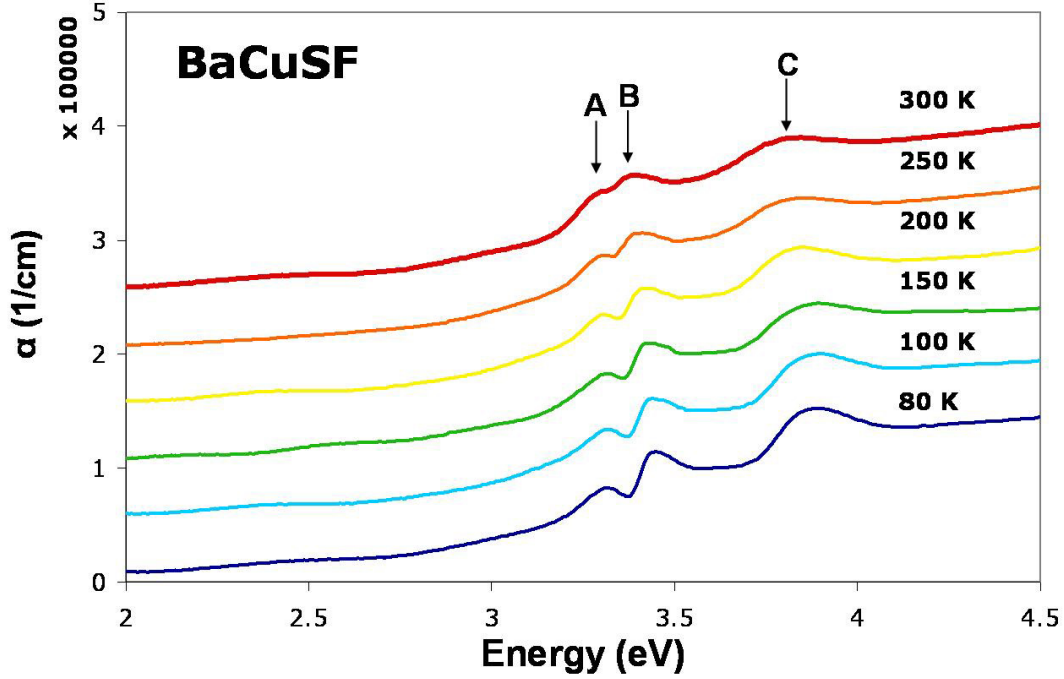


Figure 12: Absorption spectra for a thin film of BaCuSF grown on an MgO substrate. Spectra were taken at a range of temperatures from 300 degrees Kelvin down to 80 degrees Kelvin. The spectrum at each temperature is shifted vertically for clarity. (Sample showing red luminescence, $d = 320$ nm)

as

$$E_{gap}(T) = E_{gap}(0) + A \left(\frac{2}{e^{\frac{\hbar\Omega}{k_B T}} - 1} + 1 \right) \quad (8)$$

. Where A is a temperature-independent constant, k_B is Boltzmann constant, and $\hbar\Omega$ represents an average phonon energy [4]. There are two factors that contribute to the bandgap shift with temperature. As the temperature decreases the lattice constant decreases and shifts the bandgap to higher energies. The other factor that plays into the above equation is the average phonon energy that is available at a given temperature. I used Mathematica to fit the exciton peaks in BaCuSeF and BaCuSF and the bandgap of BaCuTeF. Fig. 14 shows an example fit and table 1 shows the parameters that produced the best fit for each set of data.

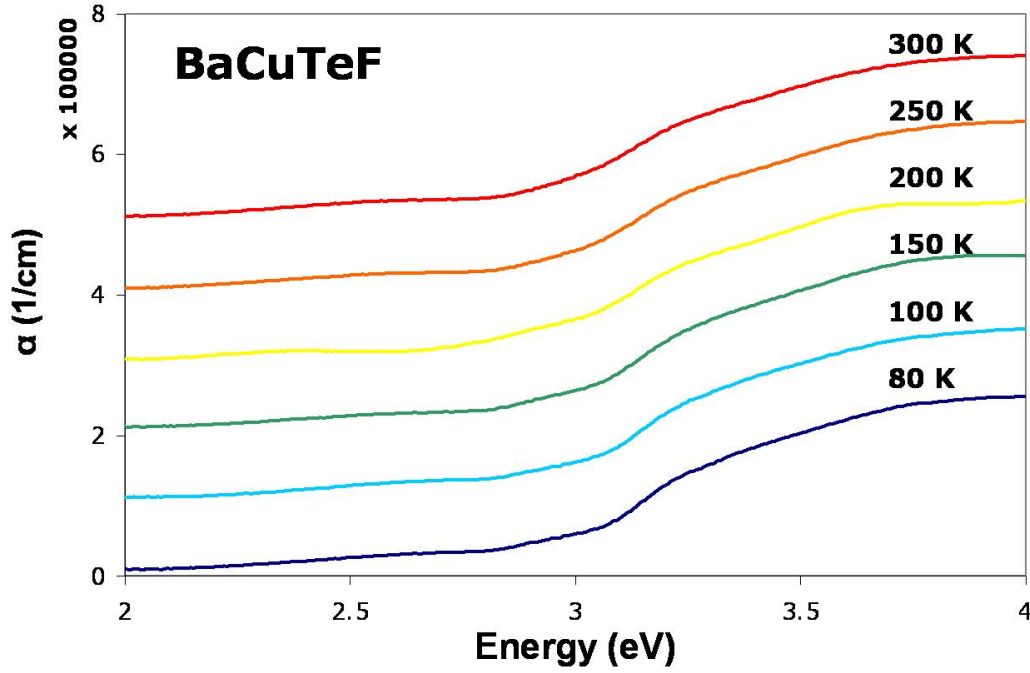


Figure 13: Absorption spectra for a thin film of BaCuTeF grown on an MgO substrate. Spectra were taken at a range of temperatures from 300 degrees Kelvin down to 80 degrees Kelvin. The spectrum at each temperature is shifted vertically for clarity. (Sample #39, $d = 150$ nm)

The quality of the sample plays an important role in whether or not exciton features will be observed. Fig. 15 shows absorption spectra for two different samples of BaCuSF. One was grown on a MgO producing a crystalline film. The second sample was grown on a SiO₂ substrate producing an amorphous film. The crystalline film shows three distinct peaks while the amorphous film only shows one clear peak. The conclusion from this is that a more crystalline, higher quality sample will show more distinct exciton features.

It would be reasonable to suspect that the reason excitons were not observed in BaCuTeF samples was caused by a lack of quality samples. The problem with that statement is that BaCuTeF samples were the highest quality of all the samples presented here. Fig. 16 shows x-ray diffraction measurements for the BaCuSeF and BaCuTeF samples showing that

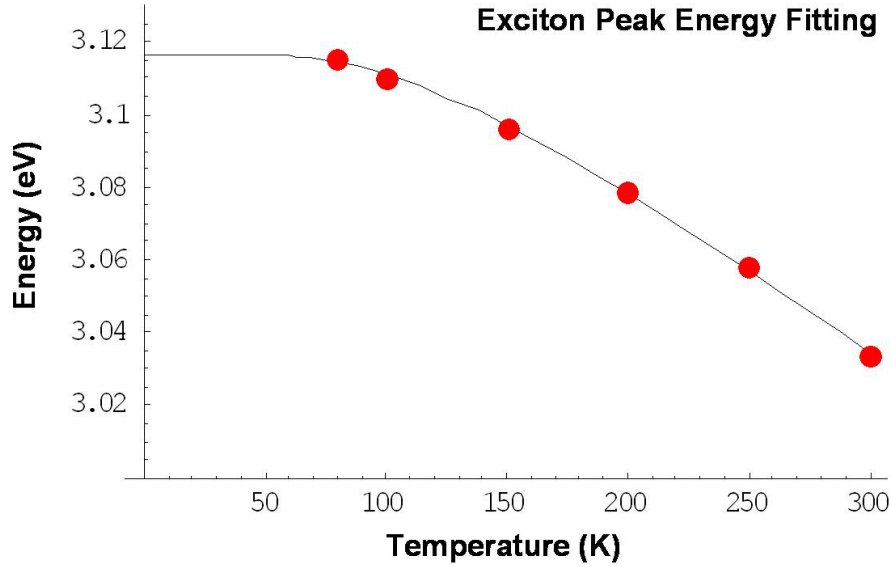


Figure 14: Example fit of exciton peak dependence on temperature. These data points correspond to BaCuSeF peak A.

both films where highly oriented crystalline films. One possible explanation for the lack of excitons in BaCuTeF could be the presence of imperfections on a scale that is not noticeable on x-ray diffraction patterns. BaCuTeF films show higher conductivity than BaCuSeF films and the likely cause of this increased conductivity is impurities in the crystal. The same defects that cause increased conductivity could also be the reason excitons are not observed.

Absorption spectra from samples of BaCuSeF and BaCuSF both show excitonic peaks at

Data Set	A	$\Theta = \frac{\hbar\Omega}{k_B}$	$E_{gap}(0)$
BaCuSeF Peak A	-0.0900	347	3.20
BaCuSeF Peak B	-0.0396	227	3.29
BaCuSF Peak A	-1.69	1697	4.98
BaCuSF Peak B	-0.0423	236	3.50
BaCuSF Peak C	-0.101	327	3.98
BaCuTeF Bandgap	-0.0398	263	3.03

Table 1: Results of fitting exciton data to temperature dependence equation.

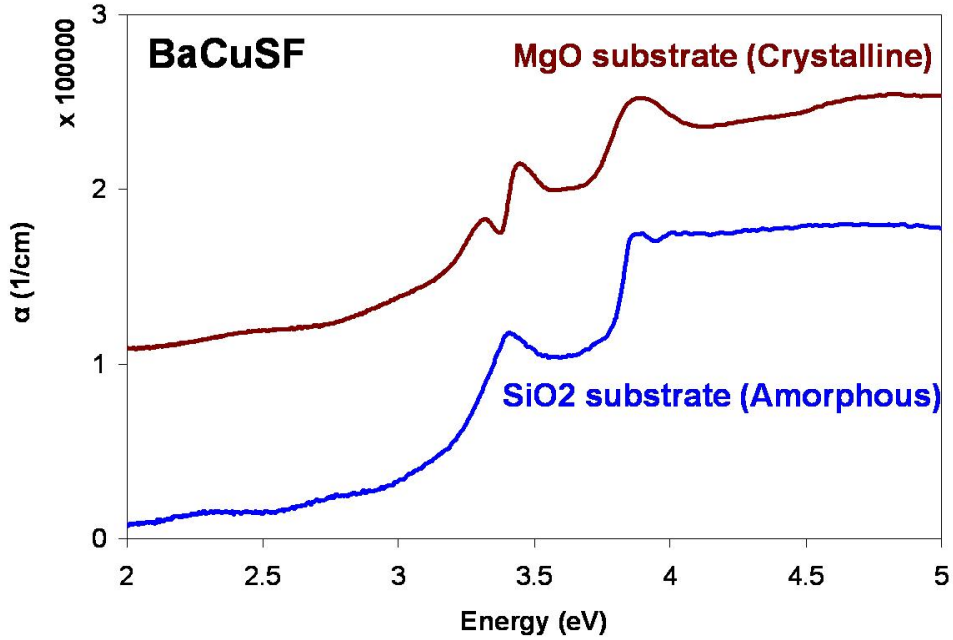


Figure 15: Absorption spectra for two different samples of BaCuSF. The crystalline sample grown on an MgO substrate shows three excitonic peaks. The amorphous sample grown on SiO₂ only displays one excitonic peak. Both spectra were taken at 80 K and the vertical shift is artificial.

room temperature, which means that the binding energy of these excitons is larger than 25 meV. There are a number of ways to model the multiple peaks displayed in these absorption spectra. For example, the two exciton peaks in BaCuSeF could be modeled in two possible ways, either the two peaks correspond to two separate exciton series where both are the $n = 1$ peak or both correspond to a single series where one peak is the $n = 1$ peak and the other is the $n = 2$ peak. The absorption of an $n = 2$ peak will be significantly smaller than the $n = 1$ peak for that same series because the intensity of the exciton peaks falls off like n^{-3} [13]. The two peaks observed in BaCuSeF are of nearly equal amplitude, so the likely model is that the two peaks are from two separate $n = 1$ exciton bands, where these two bands are spin orbit split. Hosono makes a similar argument about spin orbit splitting based off absorption spectra for LnCuOCh films [10].

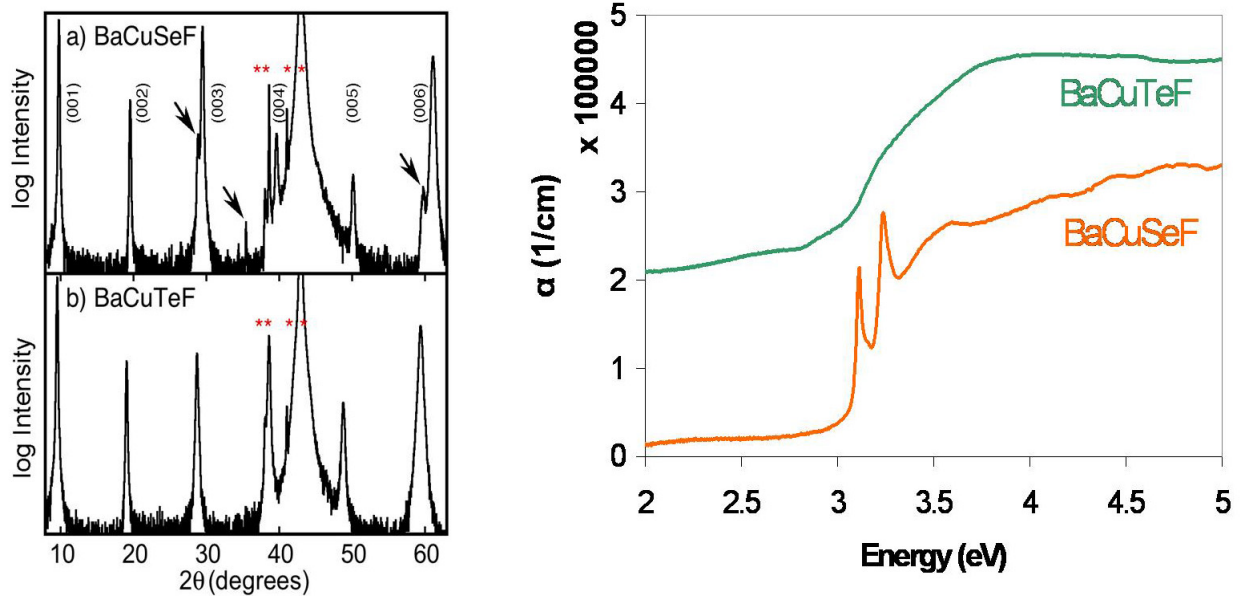


Figure 16: X-ray diffraction and absorption spectra for BaCuSeF and BaCuTeF samples. The x-ray patterns clearly show (001), (002), (003), etc peaks for both samples indicating that the materials are well oriented and highly crystalline. The peaks marked with * are MgO substrate reflections. The absorption spectrum for BaCuSeF shows two sharp excitonic peaks, while the BaCuTeF spectrum does not show any peaks. Both absorption spectra were taken at 80 K and the vertical shift is artificial.

Trying to find the binding energy if each peak corresponds to a different exciton series is difficult because there is not enough information to solve equations 1 or 4. I know the energy of the $n = 1$ exciton peak, but I do not know the energy of the bandgap or the binding energy. If I assume that one peak corresponds to the $n = 1$ peak and another corresponds to the $n = 2$ peak I have two equations, one for $n = 1$ and one for $n = 2$. Combining these two equations I can solve for both the binding energy and the bandgap. The results of this process are shown in table 2. Binding energies of 100 meV or larger are comparable to excitons observed in insulating alkali halide compounds. I would expect the binding energy to be closer to ZnO, with a binding energy near 40 meV, making the values of 33.3 meV and 36.6 the most reasonable.

I can say with one hundred percent certainty that the binding energy of the excitons in

Material	$n = 1$ (eV)	$n = 2$ (eV)	$R^*(3D)$ (meV)	$R^*(2D)$ (meV)
BaCuSeF	3.12	3.24	160	33.8
BaCuSF	3.31	3.44	173	36.6
BaCuSF	3.31	3.88	760	160

Table 2: Binding energies calculated assuming that multiple peaks correspond to different n values of the same exciton series. This is most likely an incorrect assumption because generally only the $n = 1$ peak of a series will be visible.

both BaCuSeF and BaCuSF is larger than 25 meV. This conclusion comes from the fact that the excitons are visible at room temperature and must have a binding energy larger than $k_B T$ at 300 K. One strategy for determining the binding energy is to heat up the sample until the exciton disappears. The exciton should disappear when $k_B T$ is equal to the binding energy of the exciton. I attempted this with a BaCuSF film, but unfortunately I was only able to heat the film up to 100°C. This was not hot enough to make the exciton disappear. I can conclude that for that particular BaCuSF film the binding energy is larger than 31 meV, $k_B T$ at 300 K. The results of the 100°C measurement is displayed in Fig. 17. A group at North Carolina State did some work fitting the absorption spectra to find binding energies of multiple exciton peaks [14]. This model is based off work by Sturge [15] and Elliot [13]. When I looked into this process I noticed that the three did not appear consistent and I never resolved this issue.

5 Conclusion

BaCuChF is a material that was originally developed for applications in transparent electronics. There is currently a lack of p-type transparent semiconductors and BaCuChF is a material that that could fill this need. Room temperature excitons were observed in BaCuSeF and BaCuSF. These features make these materials promising candidates for applications in optoelectronics where they could be used to build LEDs or laser diodes that produce ultraviolet light. The crystal quality of the film played an important role in pro-

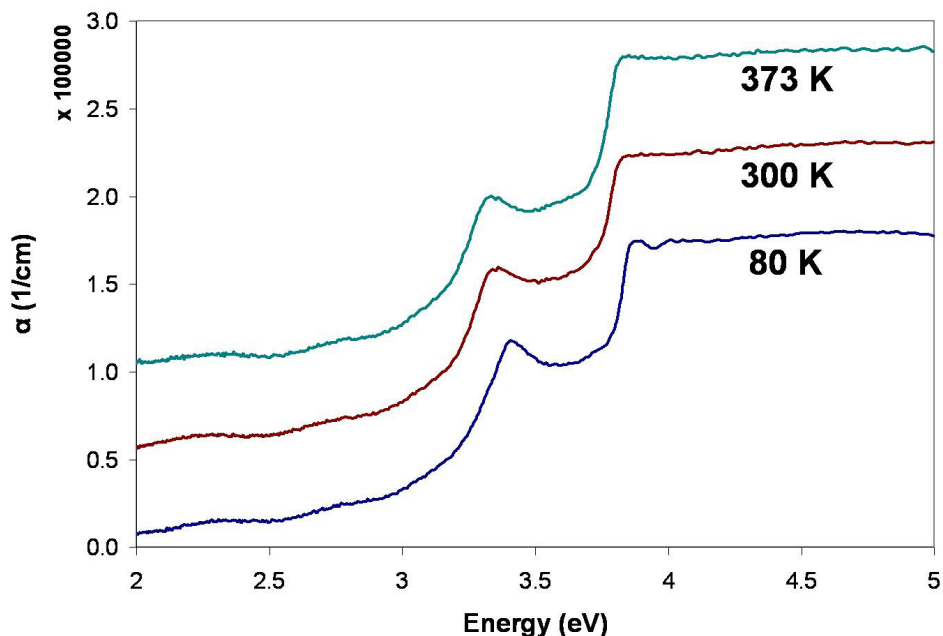


Figure 17: Absorption spectra for BaCuSF taken up to 373 K. The goal was to find the exciton binding energy by heating up the film to the point where the exciton disappears. Unfortunately, 373 K was the limit of my experimental apparatus and was not hot enough to find the exciton binding energy.

ducing sharp exciton features. Crystalline films grown on MgO substrates produced more distinct exciton features than amorphous films grown on SiO₂. BaCuTeF did not show excitons at any temperature even though the BaCuTeF film was highly crystalline and well oriented. There are multiple ways to interpret the exciton peaks and calculate the binding energy of the excitons, with values ranging from 33-760 meV. The binding energy must be larger than 25 meV because the excitons are visible at room temperature, but no upper limit was found.

6 Acknowledgments

I would like to thank my research advisor Janet Tate for helping me out in about a thousand different ways. She taught me everything I needed to know along the way whether it was

solid state physics or spelling and grammar. I cannot thank her enough for all the time and effort she put in to make this project happen.

The second person I would like to thank is David McIntyre. The primary tool I used for measuring excitons was transmission spectra and he was kind enough to let me use his spectrometer to make that happen. He was willing to discuss any particular problem I was having and always did so in a clear and helpful manner.

The final person I would like to thank is Robert Kykyneshi. Robert is a graduate student who is also in Janet Tate's research group, and he is the person who fabricated all the films that I made measurements on. He also is the person who showed me the ropes when I first started, and I am grateful for all the help he gave me along the way.

A The hydrogen atom in two dimensions

The derivation of the two dimensional hydrogen atom is very similar to solving the hydrogen atom in three dimensions. Because of this fact I was able to use Ken Krane's notes from the Central Forces Paradigm as a general guide. The starting point for this derivation will be Schrödinger's equation.

$$\left[-\frac{\hbar^2}{2\mu} \nabla^2 + V(r) \right] \psi(r, \phi) = E\psi(r, \phi) \quad (9)$$

It will be useful to work in polar coordinates (r, ϕ) for this problem. I will start with the Laplacian in Cartesian coordinates (x, y) and will use the chain rule to change to polar coordinates.

$$\nabla^2 = \frac{\partial^2}{\partial x^2} + \frac{\partial^2}{\partial y^2} \quad (10)$$

Chain rule:

$$\frac{\partial}{\partial x} = \frac{\partial r}{\partial x} \frac{\partial}{\partial r} + \frac{\partial \phi}{\partial x} \frac{\partial}{\partial \phi} \quad (11)$$

$$\frac{\partial}{\partial y} = \frac{\partial r}{\partial y} \frac{\partial}{\partial r} + \frac{\partial \phi}{\partial y} \frac{\partial}{\partial \phi} \quad (12)$$

The polar coordinates can be related to the Cartesian coordinates in the following way and all that is required is to take partial derivatives and plug them into the chain rule formula.

$$r = \sqrt{x^2 + y^2} \quad (13)$$

$$\phi = \arctan \frac{y}{x} \quad (14)$$

Combining all this information the Laplacian can be written in polar coordinates as

$$\nabla^2 = \frac{\partial^2}{\partial r^2} + \frac{1}{r} \frac{\partial}{\partial r} + \frac{1}{r^2} \frac{\partial^2}{\partial \phi^2} \quad (15)$$

. Plugging this into Schrödinger's equation gives this equation for a 2D hydrogen atom.

$$\left[-\frac{\hbar^2}{2\mu} \left(\frac{\partial^2}{\partial r^2} + \frac{1}{r} \frac{\partial}{\partial r} + \frac{1}{r^2} \frac{\partial^2}{\partial \phi^2} \right) + V(r) \right] \psi(r, \phi) = E\psi(r, \phi) \quad (16)$$

$$V(r) = -\frac{Ze^2}{4\pi\epsilon_0 r} \quad (17)$$

Combining these two expressions produces:

$$\left[-\frac{\hbar^2}{2\mu} \left(\frac{\partial^2}{\partial r^2} + \frac{1}{r} \frac{\partial}{\partial r} + \frac{1}{r^2} \frac{\partial^2}{\partial \phi^2} \right) - \frac{Ze^2}{4\pi\epsilon_0 r} \right] \psi(r, \phi) = E\psi(r, \phi) \quad (18)$$

To solve this equation I will use the separation of variables technique which assumes that the solution can be written as a product of functions each dependent upon only one variable.

$$\psi(r, \phi) = R(r)\Phi(\phi) \quad (19)$$

$$\left[-\frac{\hbar^2}{2\mu} \left(\frac{\partial^2}{\partial r^2} + \frac{1}{r} \frac{\partial}{\partial r} + \frac{1}{r^2} \frac{\partial^2}{\partial \phi^2} \right) - \frac{Ze^2}{4\pi\epsilon_0 r} \right] R\Phi = ER\Phi \quad (20)$$

$$-\frac{\hbar^2}{2\mu} \left(\frac{\partial^2 R\Phi}{\partial r^2} + \frac{1}{r} \frac{\partial R\Phi}{\partial r} + \frac{1}{r^2} \frac{\partial^2 R\Phi}{\partial \phi^2} \right) - \frac{Ze^2}{4\pi\epsilon_0 r} R\Phi = ER\Phi \quad (21)$$

$$-\frac{\hbar^2}{2\mu} \left(R''\Phi + \frac{1}{r} R'\Phi + \frac{1}{r^2} R\Phi'' \right) - \frac{Ze^2}{4\pi\epsilon_0 r} R\Phi = ER\Phi \quad (22)$$

Divide both sides by $R\Phi$

$$-\frac{\hbar^2}{2\mu} \left(\frac{R''}{R} + \frac{R'}{rR} + \frac{1}{r^2} \frac{\Phi''}{\Phi} \right) - \frac{Ze^2}{4\pi\epsilon_0 r} = E \quad (23)$$

$$-\frac{\hbar^2}{2\mu} \left(\frac{R''}{R} + \frac{R'}{rR} + \frac{1}{r^2} \frac{\Phi''}{\Phi} \right) - \frac{Ze^2}{4\pi\epsilon_0 r} - E = 0 \quad (24)$$

Multiply by r^2

$$-\frac{\hbar^2}{2\mu} \frac{\Phi''}{\Phi} = \frac{\hbar^2}{2\mu} \left(r^2 \frac{R''}{R} + r \frac{R'}{R} \right) + r \frac{Ze^2}{4\pi\epsilon_0} + r^2 E \quad (25)$$

$$-\frac{\Phi''}{\Phi} = r^2 \frac{R''}{R} + r \frac{R'}{R} + \frac{2\mu}{\hbar^2} r^2 \left(\frac{Ze^2}{4\pi\epsilon_0 r} + E \right) \quad (26)$$

Set both sides equal to an integration constant ℓ^2 . This leaves two single variable differential equations. The angular equation is simple to solve and does not differ from the three dimensional case.

$$-\frac{\Phi''}{\Phi} = \ell^2 \quad (27)$$

$$\Phi(\phi) = e^{i\ell\phi} \quad (28)$$

This leaves the radial equation to be solved.

$$r^2 \frac{R''}{R} + r \frac{R'}{R} + \frac{2\mu}{\hbar^2} r^2 \left(\frac{Ze^2}{4\pi\epsilon_0 r} + E \right) = \ell^2 \quad (29)$$

Divide by r^2 and multiply by R

$$R'' + \frac{R'}{r} + \frac{2\mu}{\hbar^2} \left(\frac{Ze^2}{4\pi\epsilon_0 r} + E \right) R - \frac{\ell^2}{r^2} R = 0 \quad (30)$$

To solve this equation I will look at the limiting cases of the solution. For very large r values the r^{-1} and r^{-2} terms can be neglected leaving the following equation.

$$R'' + \frac{2\mu ER}{\hbar^2} = 0 \quad (31)$$

The solution to this formula is $R = e^{-br}$ where $b = \sqrt{\frac{2\mu E}{\hbar^2}}$. The other limiting case to examine is when r is very small. For very small r the radial equation reduces to the following.

$$R'' + \frac{R'}{r} - \frac{\ell^2}{r^2}R = 0 \quad (32)$$

This equation can be solved assuming a polynomial solution $R = r^q$.

$$q(q-1)r^{q-2} + qr^{q-2} - \ell^2r^{q-2} = 0 \quad (33)$$

$$q(q-1) + q - \ell^2 = 0 \quad (34)$$

$$q = \pm\ell \quad (35)$$

The solution $r^{-\ell}$ blows up at small r so I will discard this solution and only use the solution $R = r^\ell$. Combining these two limiting cases with an additional function $H(r)$ produces a radial equation of the form:

$$R(r) = r^\ell e^{-\ell} H(r) \quad (36)$$

$$R' = \ell r^{\ell-1} e^{-br} H - br^\ell e^{-br} H + r^\ell e^{-br} H' \quad (37)$$

$$R'' = \ell(\ell-1)r^{\ell-2} e^{-br} H + b^2 r^\ell e^{-br} H + r^\ell e^{-br} H'' - 2\ell br^{\ell-1} e^{-br} H + 2\ell r^{\ell-1} e^{-br} H' - 2br^\ell e^{-br} H' \quad (38)$$

Plugging these derivatives into the radial equation and combining terms produces the following equation.

$$rH'' + (2\ell - ebr + 1)H' + \left(\frac{b^2 Z e^2}{E4\pi\epsilon_0} - 2\ell b - b \right) H = 0 \quad (39)$$

To find the form of the function H I will assume a series solution where H has the form:

$$H = \sum_{n=0}^{\infty} c_n r^n \quad (40)$$

$$H' = \sum_{n=0}^{\infty} n c_n r^{n-1} \quad (41)$$

$$H'' = \sum_{n=0}^{\infty} n(n-1) c_n r^{n-2} \quad (42)$$

Plugging in these derivatives and combining like terms produces:

$$(n-1+2\ell+1) \sum_{n=0}^{\infty} c_n n r^{n-1} + \left(\frac{b^2 Z e^2}{E4\pi\epsilon_0} - 2\ell b - b - 2bn \right) \sum_{n=0}^{\infty} c_n r^n = 0 \quad (43)$$

The goal here is to find a recursion relation for the coefficients c_n . I have a power series in r that must equal zero for all values of r , which implies that the coefficient of each power of r must equal zero. Plugging in $n+1$ for n in the first term of the previous equation makes the powers of r equal in the two terms and I can then equate the coefficients to find a recursion relation.

$$(n+2\ell+1) \sum_{n=-1}^{\infty} c_{n+1} (n+1) r^n + \left(\frac{b^2 Z e^2}{E4\pi\epsilon_0} - 2\ell b - b - 2bn \right) \sum_{n=0}^{\infty} c_n r^n = 0 \quad (44)$$

$$(n+2\ell+1)(n+1)c_{n+1} + \left(\frac{b^2 Z e^2}{E4\pi\epsilon_0} - 2\ell b - b - 2bn \right) c_n = 0 \quad (45)$$

$$c_{n+1} = \frac{c_n \left(b(2\ell + 2n + 1) - \frac{b^2 Z e^2}{E 4\pi\epsilon_0} \right)}{(n + 2\ell + 1)(n + 1)} \quad (46)$$

This is a recursion relation for the coefficients of the wave function that solves the radial part of the two dimensional hydrogen atom. For these functions to remain finite we can add an additional limitation that the sequence must terminate at some c_n . For this to happen the term in the numerator must go to zero.

$$2\ell + 2n + 1 - \frac{bZ e^2}{E 4\pi\epsilon_0} = 0 \quad (47)$$

Because both n and ℓ are integers I can say that the quantity $\frac{b^2 Z e^2}{E 4\pi\epsilon_0}$ must equal an odd integer.

$$\frac{bZ e^2}{E 4\pi\epsilon_0} = 2n - 1 \quad (48)$$

Plug in what b equals and solve for E .

$$E = \frac{Z^2 e^4 \mu}{\hbar^2 (4\pi\epsilon_0)^2 (n - \frac{1}{2})} \quad (49)$$

This is the energy spacing for a hydrogen atom confined to two dimensions. All the constants combine to equal the familiar value of 13.6 eV and the only real difference comes from the $(n - \frac{1}{2})^2$ term. Further information on the 2D hydrogen atom can be found by Yang [16].

References

- [1] John F. Wager. APPLIED PHYSICS: Transparent Electronics. *Science*, 300(5623):1245–1246, 2003.
- [2] R. L. Hoffman, B. J. Norris, and J. F. Wager. Zno-based transparent thin-film transistors. *Applied Physics Letters*, 82(5):733–735, 2003.
- [3] Charles Kittel. *Introduction to solid state physics, 8th edition*. John Wiley and Sons, Inc, 2005.
- [4] Peter Yu and Manuel Cardona. *Fundamentals of Semiconductors, 3rd edition*. Springer Berlin Heidelberg New York, 2005.
- [5] Gregory H. Wannier. The structure of electronic excitation levels in insulating crystals. *Phys. Rev.*, 52(3):191–197, Aug 1937.
- [6] A. D. Draeseke, D. A. Keszler, H. Yanagi, S. Park, and J. Tate. P-type conductivity in transparent oxides and sulfide fluorides. *Journal of Solid State Chemistry*, 175(1):34–38, 2003.
- [7] Hiroshi Yanagi, Janet Tate, Sangmoon Park, Cheol-Hee Park, and Douglas A. Keszler. p-type conductivity in wide-band-gap bacruf ($q = s, se$). *Applied Physics Letters*, 82(17):2814–2816, 2003.
- [8] M. Bayer, S. N. Walck, T. L. Reinecke, and A. Forchel. Exciton binding energies and diamagnetic shifts in semiconductor quantum wires and quantum dots. *Phys. Rev. B*, 57(11):6584–6591, Mar 1998.
- [9] K. Ueda, S. Inoue, H. Hosono, N. Sarukura, and M. Hirano. Room-temperature excitons in wide-gap layered-oxysulfide semiconductor: Luos. *Applied Physics Letters*, 78(16):2333–2335, 2001.

- [10] Kazushige Ueda, Hidenori Hiramatsu, Hiromichi Ohta, Masahiro Hirano, Toshio Kamiya, and Hideo Hosono. Single-atomic-layered quantum wells built in wide-gap semiconductors LnCuOCh (Ln = lanthanide, Ch = chalcogen). *Physical Review B (Condensed Matter and Materials Physics)*, 69(15):155305, 2004.
- [11] D. G. Thomas. The exciton spectrum of ZnO . *J. Phys. Chem. Solids*, 15:86–96, 1960.
- [12] Y. S. Park, C. W. Litton, T. C. Collins, and D. C. Reynolds. Exciton spectrum of ZnO . *Phys. Rev.*, 143(2):512–519, Mar 1966.
- [13] R. J. Elliott. Intensity of optical absorption by excitons. *Phys. Rev.*, 108(6):1384–1389, Dec 1957.
- [14] J. F. Muth, R. M. Kolbas, A. K. Sharma, S. Oktyabrsky, and J. Narayan. Excitonic structure and absorption coefficient measurements of zno single crystal epitaxial films deposited by pulsed laser deposition. *Journal of Applied Physics*, 85(11):7884–7887, 1999.
- [15] M. D. Sturge. Optical absorption of gallium arsenide between 0.6 and 2.75 eV. *Phys. Rev.*, 127(3):768–773, Aug 1962.
- [16] X. L. Yang, S. H. Guo, F. T. Chan, K. W. Wong, and W. Y. Ching. Analytic solution of a two-dimensional hydrogen atom. i. nonrelativistic theory. *Phys. Rev. A*, 43(3):1186–1196, Feb 1991.